www.nature.com/scientificreports

scientific reports

OPEN

Innovative application of graphene nanoplatelet-based ionanofluids as heat transfer fluid in hybrid photovoltaic-thermal solar collectors

I. Moulefera[1,2], J. J. Delgado Marín[1]✉, A. Cascales[1], M. G. Montalbán[1], M. Alarcón[3] & G. Víllora[1]

The ongoing pursuit of efficient solar thermal energy systems has driven significant interest in the development of advanced nanofluids, particularly those utilizing carbon-based nanostructures such as graphene nanoplatelets (GNP) and carbon nanotubes (CNTs). These materials, when dispersed in base fluids like water or ionic liquids, have gained attention for their tunable thermophysical properties, including thermal conductivity, viscosity, and specific heat capacity. This has positioned them as promising candidates for enhancing the thermal performance of solar collectors. However, literature examining direct experimental comparisons between the thermophysical behavior of GNP-based and CNT-based nanofluids, particularly in both water and ionic liquid media, remains sparse. Similarly, studies evaluating how such nanofluids affect the overall efficiency of solar collectors are limited and fragmented. This study investigates, for the first time, the application of GNP-based ionanofluids (INFs) in commercial hybrid photovoltaic-thermal (PVT) solar collectors. INFs were prepared using GNP and 1-ethyl-3-methylimidazolium acetate ([Emim] Ac) ionic liquid. Their thermophysical properties, including density, viscosity, thermal conductivity, and specific heat capacity, were comprehensively characterized. Long-term stability was also assessed to ensure consistent performance over time. Comparative tests with water and pure ionic liquid as base fluids revealed that INFs exhibited a significantly higher temperature rise within the collector, attributed to their lower specific heat capacity. This resulted in an exergy efficiency improvement of over 5% compared to the ionic liquid alone, underscoring the potential of INFs as advanced heat transfer fluids for high-temperature solar systems. These findings highlight the novelty of using GNP-based INFs in solar applications and pave the way for future research in optimizing nanofluid compositions for renewable energy systems.

Keywords Ionic liquid, Ionanofluids, Graphene nanoplatelets, Photovoltaic-thermal systems (PVT), Thermal conductivity, Heat transfer fluids, Solar collectors, Exergy efficiency

The industrial revolution was a pivotal moment in human history, ushering in an era of significant societal progress characterized by rapid economic growth, enhanced living standards, and groundbreaking technological advancements. This period also saw the global spread of industrialization. However, these advancements brought with them a series of challenges that now threaten to hinder future progress. Among these challenges are global warming, increased waste production, and direct environmental pollution, affecting the quality of air, water, and soil[1]. Therefore, it becomes imperative to harness the legacy of the industrial revolution to reduce the consumption of other finite energy resources, particularly fossil fuels, which are not only depleting but also significant contributors to these pressing environmental issues[1–3].

[1]Chemical Engineering Department, Faculty of Chemistry, Regional Campus of International Excellence “Campus Mare Nostrum”, University of Murcia, 30071 Murcia, Spain. [2]Department of Chemical Engineering, Faculty of Science, University of Málaga, Andalucía TECH, 29071 Málaga, Spain. [3]Electromagnetism and Electronics Department, International Campus of Excellence in the European Context (CEIR) Campus Mare Nostrum, University of Murcia, Murcia, Spain. ✉email: josejavier.delgado@um.es

Solar thermal energy represents a promising alternative source of energy[3,4]. The energy the sun emits onto Earth daily is ten thousand times greater than the energy consumed worldwide in a single day. Solar thermal systems harness the energy received from the sun to heat a heat transfer fluid, store it, and then transfer it to the working fluid for subsequent use at various points of consumption. Over the past few years, the use of solar energy in solar thermal installations has experienced a significant increase[1,5–8]. This growth is driven by the need to enhance environmental sustainability and preserve the future of our planet through the use of renewable energy sources[1,5,6]. Flat-plate solar collectors (FPSC) are widely employed in both commercial and residential settings for this purpose. These flat-plate collectors come in various types, including thermal collectors[6–9], photovoltaic collectors[5,9,10], and hybrid models, such as photovoltaic and thermal (PVT) collectors[11,12], which combine both heat and electricity generation capabilities[11].

Most solar installations involve two fluids: the heat transfer fluid and the working fluid[8,9]. Water is widely utilized as a universal fluid in various systems owing to its favorable performance and cost-effectiveness[11–13]. However, it should be noted that water can have corrosive properties and, as a thermal fluid, exhibits a relatively high vapor pressure[14,15]. The practical use of water near 100 °C can pose risks, primarily due to the potential for unintended steam generation[15,16].

However, other types of fluids, such as nanofluids[7,17–20], can be used. Nanofluids consist of nanoscale particles suspended in a base fluid and their addition produces significant changes in the thermophysical properties of the base fluid[3,17,21]. These changes include modifications to dynamic viscosity and, more importantly, thermal conductivity, which is crucial for heat transfer. The enhancement of thermal conductivity can lead to improved performance in solar collectors[3,17,21–24].

Ionanofluids (INFs) differ from nanofluids in that nanoparticles are dispersed in an ionic liquid (IL) as the base fluid[25–28]. It has been demonstrated that INFs can increase the thermal capacity of ILs without adversely affecting their thermal stability[27,29–31]. The primary properties targeted for improvement in ILs are specific heat capacity and thermal conductivity, which is why nanoparticles are added to these fluids to achieve more promising results in solar energy installations. Studies have shown that as the temperature increases, the heat capacity of INFs based on ILs containing pyridinium and imidazolium cations increases[32,33]. Furthermore, in 2003, Moens et al.[34] reported a comprehensive evaluation of ILs for use as heat transfer fluids in parabolic solar collectors, highlighting the high thermal stability of these fluids, which is crucial for such systems. They also studied the levelized electricity cost (LEC) of various fluids, concluding that ILs potentially minimize operational costs due to their low melting point.

Recently, Asleshirin et al.[35] studied and compared the thermophysical properties of INFs containing multi-walled carbon nanotubes and graphene dispersed in the IL 1-hexyl-3-methylimidazolium hexafluorophosphate ([Hmim] PF_6^-). They measured these properties experimentally and found that INFs exhibited increased thermal conductivity, heat capacity, and viscosity compared to the pure IL. Hosseinghorbani et al.[36] studied the preparation of an INF without surfactants, dispersing graphene oxide nanoparticles at mass fractions of 0.5%, 1%, and 2% (wt/wt.%) in the IL 1-butyl-3-methylimidazolium bis(trifluoromethylsulfonyl)imide ([Bmim] NTf_2^-). Using Dynamic Light Scattering (DLS), they analyzed size distribution and stability and reported a 6.5% increase in thermal conductivity and a 57% increase in heat capacity compared to the pure IL base fluid. Therefore, it was concluded that the application of INFs as heat transfer fluids in solar power plants can lead to an overall improvement in system efficiency. Additionally, they found that the maximum heat transfer coefficient was achieved with a 0.5% mass concentration, resulting in a 7.2% improvement[36].

The ongoing pursuit of efficient solar thermal energy systems has driven significant interest in the development of advanced nanofluids, particularly those utilizing carbon-based nanostructures such as graphene nanoplatelets (GNP) and carbon nanotubes (CNTs). These materials, when dispersed in base fluids like water or ILs, have gained attention for their tunable thermophysical properties, including thermal conductivity, viscosity, and specific heat capacity. This has positioned them as promising candidates for enhancing the thermal performance of solar collectors. However, the literature examining direct experimental comparisons between the thermophysical behavior of GNP-based and CNT-based nanofluids, particularly in both water and IL media, is sparse. Similarly, studies evaluating how such nanofluids affect the overall efficiency of solar collectors remain limited and fragmented.

Previous work has extensively analyzed water-based GNP and CNT nanofluids individually, evidencing that GNP often provide superior performance relative to CNTs. For instance, Sarsam et al.[37], and Alawi et al.[38], demonstrated that GNP-based nanofluids enhance thermal conductivity and solar collector thermal efficiency more effectively than CNT-based nanofluids in water. This is attributed to GNP 2D structure, which offers a larger surface area and better interaction with heat flux than the 1D cylindrical structure of CNTs. Nonetheless, other studies show that CNT-based nanofluids—particularly those containing multi-walled carbon nanotubes (MWCNTs)—exhibit significantly higher viscosity, which can hinder flow performance in practical applications[37,39]. On the other hand, MWCNTs have been shown to enhance anisotropic heat transfer due to their directional thermal conductivity[39]. The lack of comparative studies under controlled experimental conditions makes it difficult to firmly establish the relative trade-offs between GNP, single-walled carbon nanotubes (SWCNTs), and MWCNTs.

Despite the focus on water as the primary base fluid, there is growing recognition of the potential benefits of ILs due to their thermal stability and ability to reduce nanoparticle agglomeration through electrostatic stabilization. However, studies investigating IL-based carbon nanofluids are remarkably limited, with no reference in this search directly addressing their behavior in both GNP and CNT formulations for solar collectors. While some studies explore alternative base fluids such as ethylene glycol[40], the lack of cross-medium investigations represents a critical gap in understanding the full potential application of these nanofluids for high-temperature solar systems.

Functionalization to improve nanoparticle dispersion has emerged as another key focus area. Covalent modifications, such as β-alanine-treated MWCNTs or pentaethylene glycol-treated GNP, have been shown to significantly enhance thermal conductivity and stabilization while potentially mitigating viscosity increases[37–39,41–43]. Furthermore, Alawi et al. identified that chemically modified GNP in water improved convective heat transfer efficiency without clear viscosity penalties[41]. However, reductions in specific heat capacity caused by nanoparticle additions remain a persistent limitation, something that functionalization needs to fully address. This work suggests that while there is a general understanding of the advantages and limitations of carbon-based nanofluids in water, systematic investigations comparing GNP, SWCNTs, and MWCNTs across both water and IL media are missing. Such studies are crucial for balancing thermophysical property trade-offs—namely, maximizing thermal conductivity while minimizing viscosity and specific heat capacity reductions—in real-world solar collector applications. Furthermore, experimental validation of IL-based nanofluids under solar collector operating conditions, including their stability, thermal behavior, and energy efficiency performance, remains an important area of unmet need[44]. These gaps underline the need for more comprehensive research to optimize carbon-based nanofluids for solar thermal energy systems.

Nanofluids, including INFs, are considered effective in enhancing the efficiency of high and low temperature solar energy systems[45,46], as well as hybrid PVT solar systems. Das et al.[47] conducted a numerical simulation of INFs composed of a binary solution of IL + water with two dimensional MXene (Ti_3C_2) nanoparticles at various concentrations operating in a solar PVT system. They concluded that MXene-based INFs show promising potential in heat transfer applications. Shaik et al.[48] predicted the behavior of MXene-based INFs for hybrid solar photovoltaic and thermal systems by means of an Artificial Neural Network (ANN) model and Response Surface Methodology (RSM) based optimization techniques.

Innovative INFs were synthesized by GNP with the IL 1-ethyl-3-methylimidazolium acetate ([Emim] Ac). The selection of 1-ethyl-3-methylimidazolium acetate ([Emim] Ac) as the base fluid in this study is justified by its unique combination of properties that make it highly suitable for heat transfer applications. First, [Emim] Ac exhibits superior thermal stability in high-temperature operations, allowing it to operate effectively under high-temperature conditions without significant degradation[49]. Second, its low vapor pressure minimizes the risk of evaporation and ensures long-term operational stability, which is critical in thermal systems. Additionally, [Emim] Ac possesses relatively low viscosity compared to other ILs, enabling better fluidity and enhanced heat transfer performance. Importantly, [Emim] Ac also demonstrates relatively low ecotoxicity[50], making it an environmentally safer alternative to conventional fluids. Lastly, [Emim] Ac is highly compatible with GNP, facilitating effective dispersion and minimizing agglomeration, which are essential for maintaining stable INF properties.

In this study, a comprehensive characterization of the GNP-based INFs was carried out, focusing on their physicochemical and thermophysical properties, including viscosity, thermal conductivity, specific heat capacity, and long-term stability. Furthermore, their performance was evaluated through a series of tests in a PVT solar collector, comparing the efficiency of the IL and INF as working fluids with that of water. Remarkably, this work represents the first reported application of ILs and their INF derivatives in real-world operating conditions within commercial PVT systems, marking a significant advancement in the field.

Materials and methods

Materials

The IL 1-ethyl-3-methylimidazolium acetate (≥ 95% purity), [Emim] Ac, was supplied by IoLiTec (Heilbronn, Germany) and used as received. GNP were purchased from Merck (Darmstadt, Germany) and used as received. According to the supplier, GNP have a size of 5 μm, a surface area ranging from 50 to 80 $m^2\ g^{-1}$, and a molecular weight of 12.01 g mol^{-1}.

GNP characterization

Field emission scanning electron microscopy (FESEM)

The morphology of GNP was characterized using a Field Emission Scanning Electron Microscope (FESEM) with a FEI SciosTM microscope from Thermo Scientific (Waltham, MA, USA). A drop of an aqueous dispersion of 10 μg/mL GNP was set onto a silica support, dried using an infrared lamp and then coated with a 2 nm thick platinum layer.

Attenuated total reflectance Fourier transformed infrared spectroscopy (ATR-FTIR)

Infrared spectral data of GNP were acquired using attenuated total reflectance Fourier transform infrared spectroscopy (ATR-FTIR) with a Nicolet iS5 spectrometer, which was equipped with a diamond crystal ATR iD7 module from Thermo Fisher Scientific (Waltham, MA, USA). The control and processing of spectral data were performed using OMNIC V9.9.471 software. The interferograms were recorded with a resolution of 4 cm^{-1} within the spectral range of 4000–400 cm^{-1}. A zero-fill factor of 2 was applied, and Fourier transformation was carried out using the Blackman–Harris 3-term apodization function. Each measured spectrum had an average of 64 scans. Prior to each measurement, an unsampled background spectrum was collected. To acquire the spectra of the samples, 2 μL of a 0.66 mg/mL GNP aqueous dispersion were loaded onto the ATR crystal after drying under a gentle stream of nitrogen.

Preparation of INFs

Four INFs containing different mass fractions of GNP (0.005%, 0.05%, 0.25%, and 1% wt/wt.%) were prepared. For this, the required mass of GNP was initially dispersed in the required mass of IL under magnetic stirring overnight. Then, the sample was bath sonicated for 30 min at 30 °C and, finally, was probe sonicated with a

Branson 450D high power ultrasonicator at 40% amplitude with pulses of 59s ON/29s OFF for 2h. Due to the high temperature reached during ultrasonication, the experiments were carried out in an ice bath (see Fig. 1).

INF characterization

Once the INFs were obtained, their size distribution was analyzed using Dynamic Light Scattering (DLS) with a Malvern Zetasizer Nano ZSP instrument from Malvern Instruments Ltd. (Grovewood, UK). The instrument was equipped with a laser emitting at 4 mW power and at wavelength of 633 nm. This analysis determined the hydrodynamic intensity-weighted averaged diameter, known as Z-average.

The sample stability was checked using the Turbiscan®LAB™ equipment (Formulaction Inc, France) by the Multiple Light Scattering (MLS) technique. In operation, the sample dispersion is housed within a cylindrical glass cell and left there for 48 h. Illumination is provided by an electroluminescent diode emitting near-infrared light at a wavelength of 880 nm ($\lambda_{air} = 880$ nm). The Turbiscan® LAB™ employs two synchronized optical sensors: one for capturing light transmitted through the sample at 180° from the incident light (transmission sensor), and the other for detecting light that is backscattered by the sample at 45° from the incident radiation (backscattering detector)[51]. The dimensionless Turbidity Stability Index (TSI) was calculated using Eq. (1) for all the INFs[51]:

$$TSI = \sum_{t_i} \frac{\sum_{h_i} |scan_{t_i}(h_i) - scan_{t_{i-1}}(h_i)|}{H} \tag{1}$$

where H is the total sample height and $scan_{i-1}$ (h_i) and $scan_i$ (h_i) are the intensity of scanning light (BS if T < 0.2%, T otherwise) at height h_i, respectively, at time t_{i-1} and t_i.

Densities were measured using an oscillating U-tube DMA 4500 M densitometer (Anton-Paar, Graz, Austria) at the temperature range of 20–70 °C. The temperature was controlled by a Peltier system. Standard uncertainty of density is 0.05 kg m^{-3}. The measurements were done at least three times.

The refractive index was measured by a RX 5000α refractometer (ATAGO CO., Tokyo, Japan) at 589 nm sodium wavelength and temperatures from 20 to 60 °C. The standard uncertainty of refractive index is 0.0002. The measurements were carried out in triplicate at least.

Viscosities were measured using a Bohlin Visco 88 rotational viscometer (Malvern, Worcestershire, UK) with a precision of ± 0.0025 Pa s at the temperature range of 20–70 °C controlled by a thermostatic bath. The measurements were taken at least in triplicate.

Thermal conductivities were determined using a TEMPOS thermal properties analyzer (Meter, WA, USA) with the technique called hot wire at temperature range of 20–60 °C. Each sample was measured at least three times at every temperature with a precision of ± 0.0075 W m^{-1} K^{-1}. The measurements were carried out by putting the samples into a thermostatic bath at the desired temperature, ensuring that no movement was induced by using a clamp. The samples were maintained at a stable temperature until equilibrium was achieved. Subsequently, the water flow was reduced to 10% of the bath capacity to ensure that the measurements were not affected by the movement. This procedure was repeated continuously overnight, with a series of measurements taken every 30 min.

Specific heat capacity measurements were performed by Differential Scanning Calorimetry (DSC 822E, Mettler-Toledo, Ohio, USA) using an IsoStep method with sapphire as the comparison standard. Nitrogen was used to purge the system with a flow of 50 mL min^{-1}. All measurements were taken at temperatures ranging from

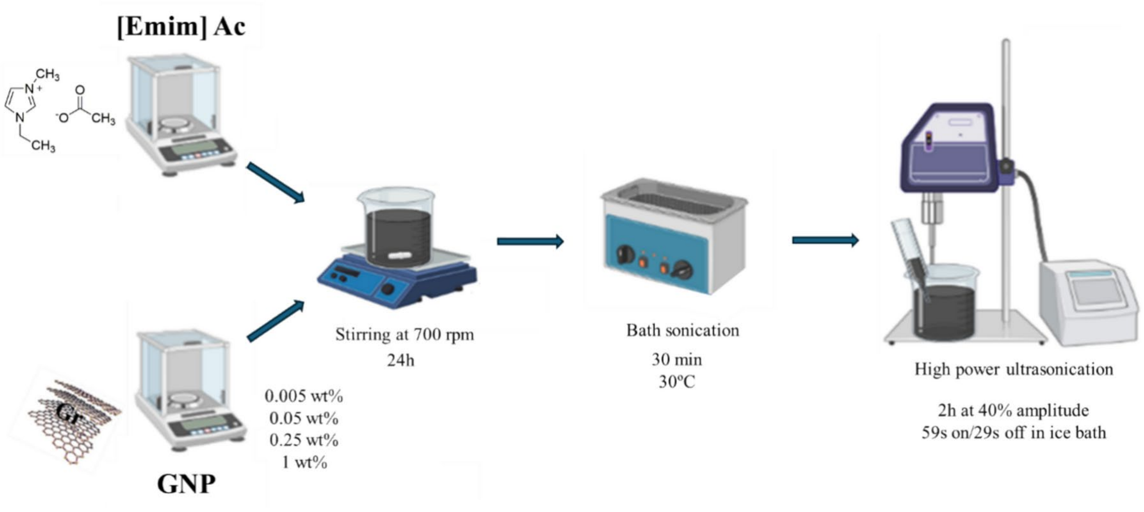

Fig. 1. Preparation method of INFs.

20 to 70 °C. The IsoStep method consists of an alternating series of isothermal steps of 2 min followed by non-isothermal steps of 2 min with heating rate of 2.5 °C/min. The measurements were taken in triplicate.

Thermal stabilities of INFs were analyzed using a TGA/DSC 1HT thermogravimetric analyzer (Mettler-Toledo, Barcelona, Spain). The samples were heated from 30 to 800 °C at a rate of 10 °C/min under a nitrogen atmosphere.

Solar collector tests

The tests were conducted in the Solar Energy Laboratory of the University of Murcia[52], equipped with different kind of solar collectors (Fig. 2). In particular, to assess the performance of the INFs, the tests were conducted in a commercial PVT solar collector[53].

The PVT solar collector used, with dimensions of 1645 × 978 × 104 mm, consists of a tempered glass cover acting as a protector, followed by a set of photovoltaic cells sealed to an absorber plate made of aluminum. This plate is connected to copper conduits through which the heat transfer fluid circulates. The final element is an insulating material made of rock wool, which serves to retain heat inside the structure. The entire assembly is inclined at 45° relative to the horizontal plane, facing South, and is enclosed within an anodized aluminum casing. In this collector, the thermal part recovers most of the solar radiation that is not used by the photovoltaic cells and acts as a cooler for the photovoltaic part of the collector. Table 1 summarizes the general specifications and the thermal and electrical characteristics of the PVT collector used.

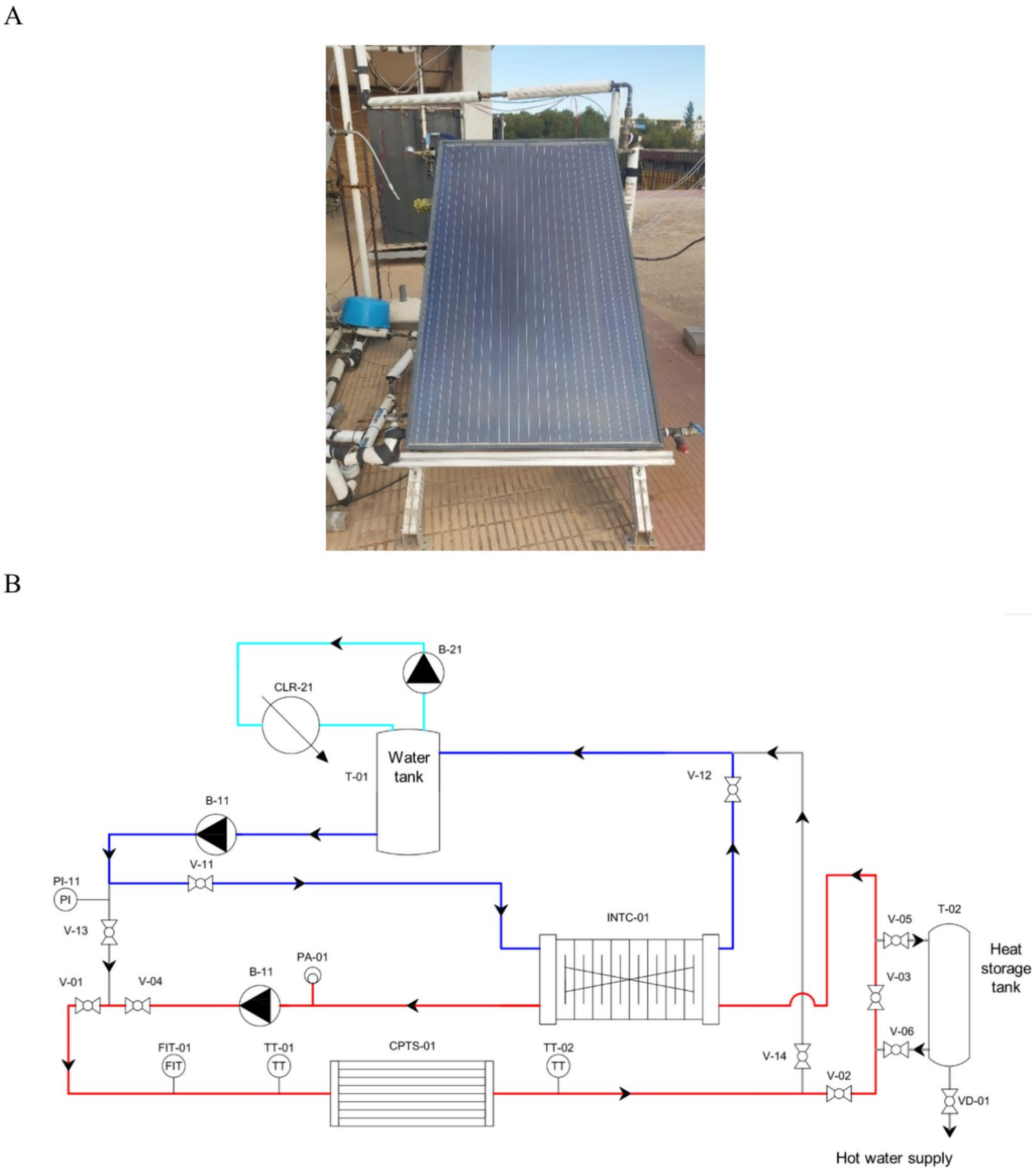

Fig. 2. (**A**) View of the PVT hybrid solar collector at the Solar Energy Laboratory of the University of Murcia. (**B**) PID Diagram of Circuits: 0 (red), primary (dark blue) and secondary (light blue) of the PVT collector.

Element	Information
General specifications	
Empty weight	46.6 kg
Cell numbers	60
Absorption plate	Copper
Thermal conductivity of the plate	385 W m^{-1} K^{-1}
Plate dimensions	1645 × 978 × 104 mm
Capture surface	1.55 m^2
External coil diameter	22 mm
Cover	Glass
Cover thickness	4 mm
Insulation	Rock wool
Insulation thickness	60 mm
Thermal specifications	
Maximum pressure	6 bar
Capacity	1.27 L
Optical performance	0.507
Coefficient of thermal losses (a1)	4.934 W m^{-2} K^{-1}
Coefficient of thermal losses (a2)	0.021 W m^{-2} K^{-1}
Stagnation temperature	148.9 °C
Electrics specifications	
Power	255 W
Open-circuit voltage (Vac)	37.9 V
Nominal voltage (Vmpp)	31.25 V
Short-circuit current (Iac)	9.30 A
Nominal current (Impp)	8.70 A
Maximum reverse current	15.0 A
Maximum system voltage	1000 V

Table 1. General specifications and thermal and electrical characteristics of the PVT solar collector.

This study conducted a comprehensive evaluation of three distinct heat transfer fluids in a PVT solar collector. The fluids under investigation included an INF containing 1% (wt/wt.%) GNP, pure IL [Emim] Ac, and water as a reference fluid. The experiments adhered strictly to the UNE-EN 12975:2022[54], standard for stationary performance tests, ensuring rigorous and comparable results. The testing protocol mandated specific environmental and operational conditions. These included maintaining hemispherical radiation levels above 700 W m^{-2}, ensuring clear sky conditions, and controlling the air velocity parallel to the absorber plane between 1 and 3 m s^{-1}[54]. The heat transfer fluid was circulated from the bottom to the top of the collector, with a venting system in place to eliminate contaminants and air bubbles[54]. Crucially, the inlet temperature was kept above the dew point to prevent condensation on the absorber. To ensure the highest level of accuracy, all measuring instruments underwent rigorous calibration prior to the experiments. This setup allowed for a direct comparison between the novel fluids (INF and IL) and the conventional water-based system, providing valuable insights into their relative performance in real-world PVT applications. It is worth noting that, while water or glycol–water mixtures are commonly used as thermal carrier fluids in such solar panels, this study explores the potential benefits of using INFs and ILs as alternative heat transfer media. This approach opens up new possibilities for enhancing the efficiency and versatility of solar thermal systems.

The first test was carried out on June 2023 with the selected INF, the second one in February 2024 using water as heat carrier fluid and the third in May 2024 using the IL [Emim] Ac. Although the tests were conducted in apparently different climatic conditions, the mild climate of Murcia (Spain) and the particular conditions of the weather, in addition to the use of the variable T^* (corrected or reduced temperature), make the results quite comparable. T^* is defined in EN 12975 Standard by Eq. (2):

$$T^* = \frac{T_m - T_{amb}}{G} \tag{2}$$

where T_m (K) is the collector mean temperature, evaluated as the average of input and output temperatures, T_{in} and T_{out} (K), respectively, T_{amb} (K) is the ambient temperature, and G (W m^{-2}) is the overall solar irradiance on the collector plane. The useful heat produced in the solar collector, Q_u (W), is accounted by Eq. (3), being $\dot{m}$ (kg s^{-1}) the mass flow rate and c_p (J kg^{-1} K^{-1}) the specific heat of the fluid.

$$Q_u = \dot{m} \cdot c_p \left(T_{out} - T_{in}\right) = \dot{m} \cdot c_p \cdot \Delta T \tag{3}$$

The thermal efficiency of the collector and the temperature rise of the fluid were analyzed in order to show the performance of the PVT collector. The thermal and electric efficiencies, denoted as η_{therm} and η_{elec}, respectively, were determined using the stationary efficiency method outlined in the UNE-EN 12975:2022 standard[54], as well as in earlier literature[55–58]. The values of the thermal and electric efficiencies are calculated using Eqs. (4) and (5), respectively:

$$\eta_{therm} = \frac{\dot{m} \cdot c_p \cdot (T_{out} - T_{in})}{A \cdot G} \tag{4}$$

$$\eta_{elec} = \frac{P}{A \cdot G} = \frac{I \cdot V}{A \cdot G} \tag{5}$$

where P is electric power (W), V is voltage (V), I is current (A), and A is the plate absorber area of the collector (m^2).

As it is known, the overall efficiency in a PVT collector is the sum between thermal and electric efficiencies. Then the total efficiency can be calculated using Eq. (6):

$$\eta_{overall} = \frac{Q_u + P}{G \cdot A} = \eta_{therm} + \eta_{elec} \tag{6}$$

Although the tests conducted may not been considered as certification ones and the standard does not consider hybrid collectors, the procedures of UNE-EN 12975:2022[54] had roughly followed for the registration and assessment of the test results where that applied. To obtain the thermal, electric and overall efficiency curve of the solar collector, sets of five minutes of data between 10:00 and 14:00 UTC (Coordinated Universal Time) hours, when irradiance was greater than 700 W m^2, have been considered.

Results and discussion

GNP characterization

Field scanning electron microscopy (FESEM)

Figure 3 shows the morphology of the GNP sample. The surface exhibits a uniform and flat overlapping pattern, indicating that the thin GNP are randomly arranged, with some layers appearing folded, as can be found in similar previous works[59–61].

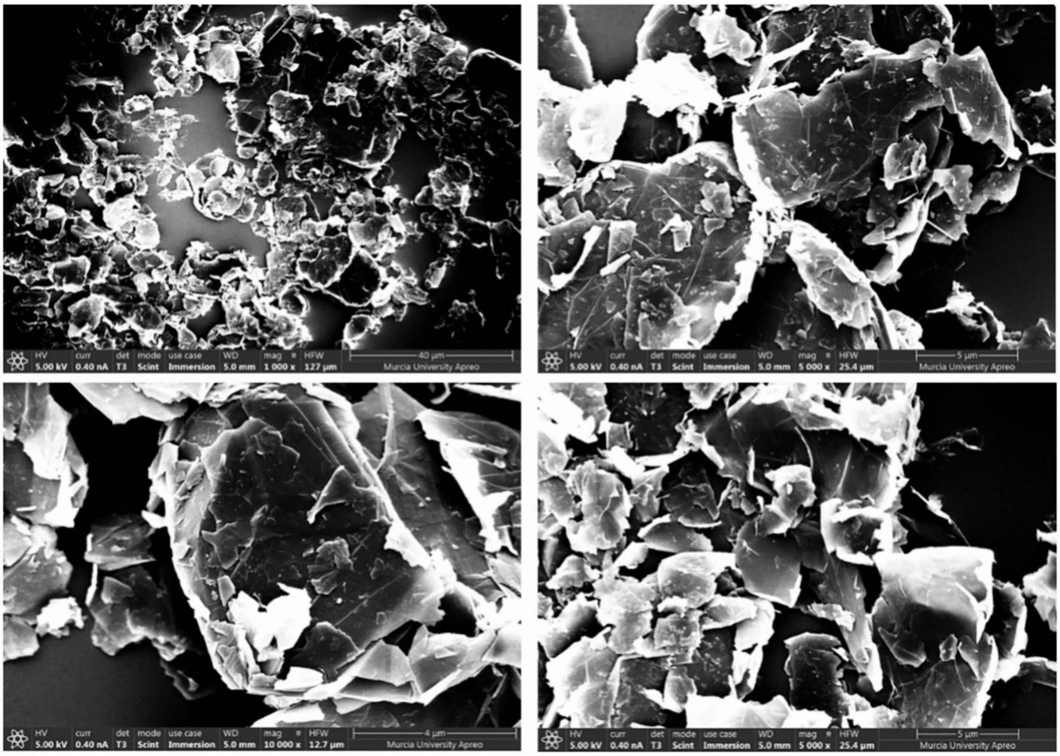

Fig. 3. FESEM micrographs of GNP.

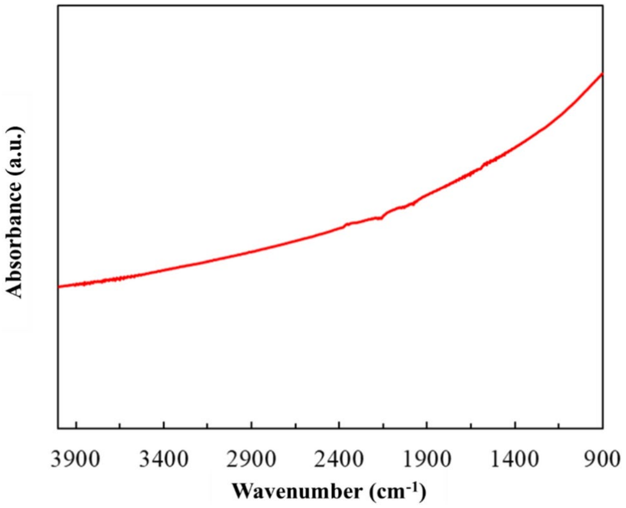

Fig. 4. *ATR-FTIR* spectra of GNP.

GNP content (wt/wt.%)	Z-Average (nm)	PDI
1%	296.5 ± 15.49	0.071 ± 0.030
0.25%	589.8 ± 14.74	1.000 ± 0.000
0.05%	410.8 ± 77.19	1.000 ± 0.000
0.005%	146.2 ± 17.20	0.165 ± 0.092

Table 2. Particle size distribution of the INFs prepared.

Attenuated total reflectance fourier transformed infrared spectroscopy (ATR-FTIR)

Figure 4 presents the ATR-FTIR of GNP. As can be seen, the figure shows a typical spectrum of the GNP. The absence of bands in the 3000–3500 cm^{-1} region indicates the lack of significant hydroxyl (–OH) groups, suggesting a low degree of oxidation in the GNP. It is important to note that the ATR-FTIR spectrum of GNP is generally simple due to the homogeneous nature of the material. The presence of additional or more bands could indicate the presence of impurities or significant surface functionalization[62–64].

INF characterization

Size distribution and stability analysis of INFs

The synthesized INFs were analyzed by DLS to determine their hydrodynamic diameter (Z-Average), polydispersity index (PDI) and the corresponding peaks of the size distribution. The results are shown in Table 2 and Fig. 5.

As can be shown in Table 2, an increase in the mass fraction of GNP from 0.005 to 0.25% seems to be correlated with an increase in the hydrodynamic diameter (expressed as Z-average) ranging from 146 to 590 nm. In the samples with 0.25% and 0.05% of GNP, the PDI reached a value of 1 which clearly indicates that the value of the Z-average is not reliable because probably more than one size population is present. However, when the GNP content increased up to 1% a much lower hydrodynamic diameter around 296 nm and PDI around 0.07 were obtained. This was the lowest value of the PDI obtained and revealed that only one size population was present. A plausible explanation for this phenomenon lies in the concentration-dependent behavior of GNP in dispersion. At lower concentrations (0.005–0.25%), GNP tend to form loose aggregates, resulting in larger hydrodynamic diameters and higher PDI values. However, as the concentration increases to 1%, the system appears to reach a critical threshold where more stable and uniform dispersions are achieved. At this higher concentration, several mechanisms may come into play:

1. Self-assembly: GNP might self-organize into more ordered structures, leading to a more uniform size distribution and consequently, a lower PDI.
2. Enhanced surface interactions: The increased concentration of GNP could promote stronger inter-particle surface interactions, potentially causing them to arrange in a configuration that minimizes their effective hydrodynamic diameter.
3. Stabilization effect: The higher GNP content may create a stabilizing effect within the dispersion, effectively preventing the formation of larger aggregates.

These combined effects at 1% concentration likely contribute to the observed reduction in hydrodynamic diameter and the significantly lower PDI value. This suggests a transition from a heterogeneous system with

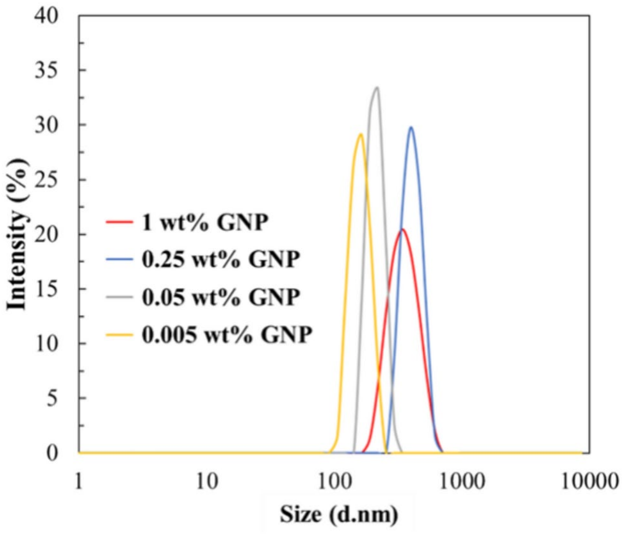

Fig. 5. Particle size distribution of the studied INFs. The percentages represent the GNP content (wt/wt).

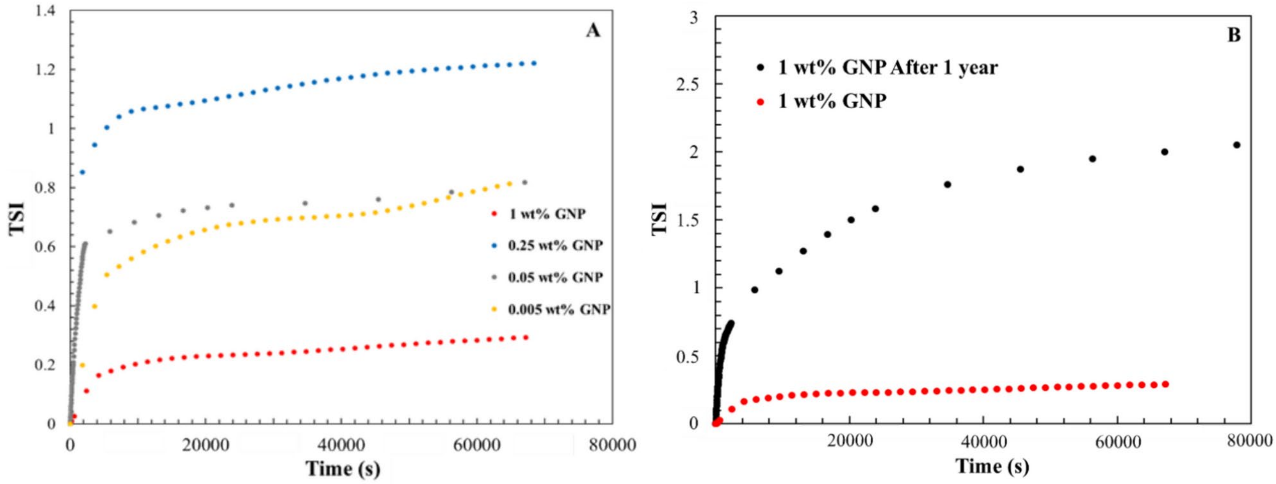

Fig. 6. Stability index of INFs over time; (**A**) INFs prepared at different concentrations of GNP; (**B**) INF at 1 wt/wt.% freshly prepared and after one year of its use in the PVT collector.

varying particle sizes at lower concentrations to a more homogeneous dispersion with a single, uniform size population at the 1% GNP content. This explanation aligns with the complex interplay between nanoparticle concentration, dispersion stability, and particle size distribution often observed in nanomaterial systems. It underscores the importance of identifying optimal concentration ranges for achieving desired material properties in GNP-based composites or dispersions.

Figure 5 illustrates the size distribution curves for the GNP dispersions at different concentrations. The data reveal a notable trend: as the concentration decreases, there is a corresponding reduction in particle size and maximum intensity. However, a more nuanced interpretation is necessary when considering the Z-average and PDI values. The data indicate that at concentrations lower than 1% GNP, aggregates with sizes exceeding those displayed in the graph have formed, despite the apparent trend towards smaller sizes at lower concentrations. This apparent contradiction between the size distribution curves and the Z-average/PDI values highlights the complexity of nanoparticle behavior in dispersions. It suggests that while lower concentrations may promote the formation of smaller particles, they may also lead to the development of larger aggregates not captured by the primary distribution curve.

The stability of the INFs obtained was assessed using Turbiscan®LAB™ over 24 h to calculate their TSI. Figure 6 summarizes how the TSI changes over time for each sample at a temperature of 25 °C. The INF prepared at a mass fraction of 1% presents a considerably lower TSI around 0.3 (Fig. 6A), suggesting a much higher stability of this sample respect to the others[65,66]. For sake of comparison, the stability of the same sample was also analyzed after one year of their used in the PVT collector (Fig. 6B). It was observed that the TSI value increased from 0.3 to 2 but still had a good stability.

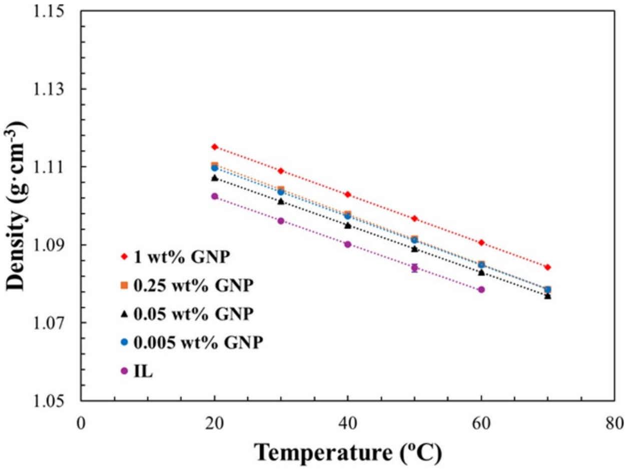

Fig. 7. Density of the INFs as function of temperature. The data related to the pure IL were sourced from the research conducted by Moulefera et al.[49].

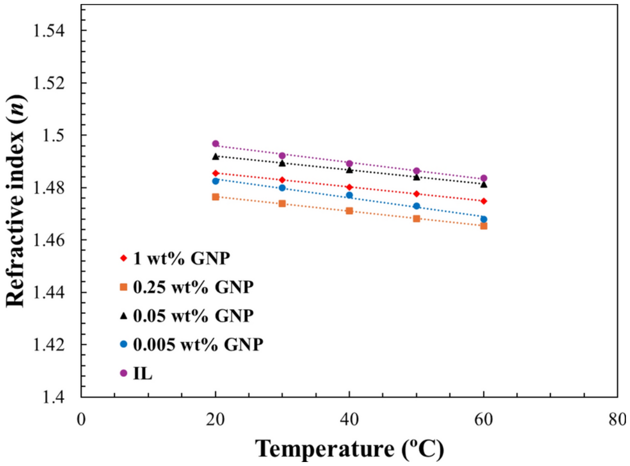

Fig. 8. Refractive index of the INFs as function of temperature. The data related to the pure IL were sourced from the research conducted by Moulefera et al.[49].

Thermophysical properties of the INFs

Density of INFs Figure 7 shows the density of INFs as a function of temperature. As expected, the density values decrease as the temperature rises. It could be also predicted that a higher mass fraction of GNP contributes to a higher density but, according to our results, the density follows the next trend: 1% > 0.25% ≈ 0.005% ≈ 0.05% > IL. The results could be explained in terms of the stability of the samples. Although the difference is less than 1%, the INFs containing 0.05% and 0.005% GNP do not follow the same trend as the others. This is likely because, along with the 0.25% GNP sample, they are the most unstable. As a result, they may precipitate within the U-tube of the density meter, leading to a density reading lower than the actual value.

The experimental density values of the studied INFs can be found in Table **S1**. They were correlated through linear regression with temperature and the fitting parameters and regression coefficients are shown in Table **S6**.

Refractive Index of INFs The refractive index (*n*) describes how the medium affects the propagation of light. Figure 8 shows the variation of the refractive index of the INFs with temperature. As expected, the refractive index decreases with temperature and with the addition of GNP for all the samples. In this case, the order of the refractive index observed was the following: 0.05% > 1% > 0.005% > 0.25%. An examination of the results reveals that the refractive index does not exhibit a consistent trend with varying concentrations of GNP in the IL. This irregularity may be attributed to the instability of the samples and the presence of aggregates, as previously discussed. Furthermore, GNP possess unique optical properties that may not scale linearly with concentration. At certain concentrations, optical phenomena such as plasmonic effects or scattering may occur, unpredictably altering the refractive index[67].

The experimental refractive index values of the INFs are shown in Table S3 They were correlated with temperature using linear regression, and the resulting fitting parameters and regression coefficients are presented in Table S2.

Viscosity of INFs Given the importance of viscosity in heat transfer systems, the viscosity of the INFs was measured as a function of temperature, and the results are shown in Fig. 9. As expected, the temperature has a strong effect on the viscosity properties, which decreases significantly with an increase in the temperature for all INFs obtained following a second-degree polynomial trend. At 20 °C the viscosity increases with increasing mass fraction of GNP. However, at higher temperatures, the differences in viscosity become less pronounced, and the values are comparable across all samples. The results obtained are in agreement with several authors that have also demonstrated that the viscosity decreases with an increase in temperature for different nanofluids[26,68,69].

As demonstrated in the figure, the incorporation of GNP into the IL matrix results in a lubricating effect, leading to a reduction in viscosity. This behavior is consistent with findings from other studies where the matrix consists of lubricating oil or glycerol[70].

The experimental viscosity values of the INFs are shown in Table S4. They were correlated using a second-degree polynomial with temperature and the fitting parameters and r-squared are collected in Table S5.

Based on the data obtained from the rotational viscometer for viscosity calculation, Newton's law is applied to the fluids to determine whether they exhibit Newtonian behavior. A fluid is classified as Newtonian if the relationship between shear stress (τ) and shear rate (γ) is linear and constant, which can be expressed by Eq. (7):

$$\tau = \eta \cdot \gamma \tag{7}$$

where η represents the dynamic viscosity of the fluid, which remains constant under specific temperature and pressure conditions for a Newtonian fluid.

In Figure S1, the shear stress is plotted against the shear rate at different temperatures for the pure IL and the INFs with varying concentrations of GNP. The linear relationship between shear stress and shear rate observed at all temperatures indicates that the dynamic viscosity is constant, confirming the Newtonian behavior of all samples tested.

Thermal conductivity of INFs Figure 10 depicts the thermal conductivity of the INFs at the temperatures studied. It is clearly observed that the thermal conductivity increases with the increase in the mass fraction of GNP, with a slight increase with temperature. These findings are consistent with the literature[26,71,72]. For example, Wang et al. reported that the thermal conductivity of INFs with the IL 1-hexyl-3-methylimidazolium tetrafluoroborate ([Hmim] BF_4^-) and graphene as nanomaterial increased by 10% with the addition of 0.03 wt.% of dispersed material[26].

The analysis of thermal conductivity as a function of temperature reveals a significant correlation with the previously observed Z-average and PDI values for different GNP concentrations. This relationship provides valuable insights into the impact of nanoparticle dispersion quality on thermal properties. The samples containing 0.25% and 0.05% GNP, which exhibited high PDI values indicative of significant aggregate formation, demonstrate the poorest linear fits of thermal conductivity with respect to temperature. This observation aligns closely with the Z-average and PDI measurements, reinforcing the link between aggregate presence and thermal behavior.

The experimental thermal conductivity values of the INFs are collected in Table **S6**. They were correlated with temperature using linear regression. The fitting parameters and regression coefficients are provided in Table S8.

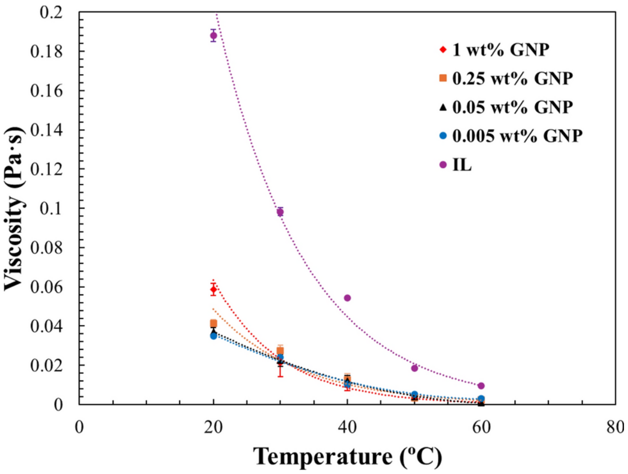

Fig. 9. Viscosity of the INFs as function of temperature. The data related to the pure ILIL were sourced from the research conducted by Moulefera et al.[49].

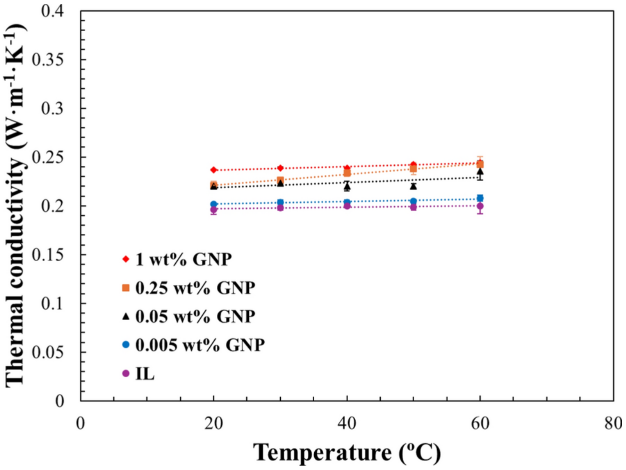

Fig. 10. Thermal conductivity of the INFs as a function of temperature. The data related to the pure IL were sourced from the research conducted by Moulefera et al.[49].

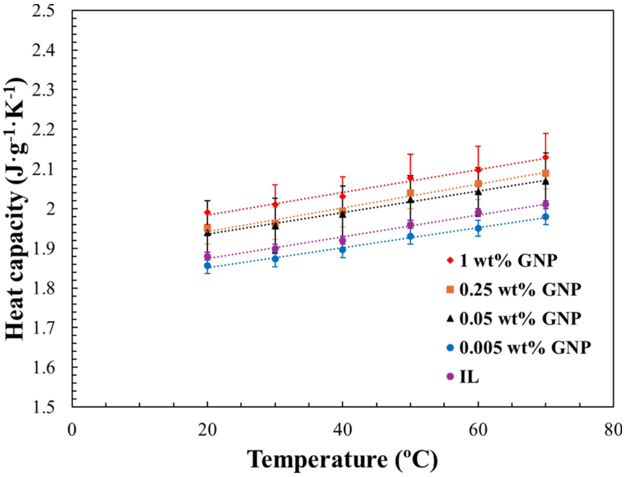

Fig. 11. Specific heat capacity of the INFs as function of temperature. The data related to the pure IL were sourced from the research conducted by Moulefera et al.[49].

Specific heat capacity of INFs To study the thermal properties of the INFs prepared, the specific heat capacities of the samples were also analyzed to determine their effect in the thermal storage equipment. Figure 11 presents the specific heat capacities (C_p) of the INFs within the investigated temperature range. It was observed that the C_p value increases with the increase of the mass fraction and with the increase of temperature as well, up to 2.15 J g^{-1} K^{-1} for the sample containing a mass fraction of 1% of GNP. The sample with the lowest concentration exhibits a specific heat capacity (Cp) lower than that of the pure IL, likely due to the measurement uncertainty accumulated during the experimental process.

The experimental specific heat capacity values of the INFs are shown in Table S8. They were correlated with temperature using linear regression, and the fitting parameters and regression coefficients are collected in Table S7.

Thermal stability of INFs Thermogravimetrical analysis was performed to investigate the thermal degradation of the INFs, a common cause of failure in heat transfer fluids in thermal systems under high-temperature conditions. The samples were heated from room temperature to 800 °C at a rate of 10 °C/min in an inert nitrogen atmosphere. Figure 12 presents the thermogravimetric curves of the INFs studied. As depicted in the figure, all the INFs exhibited similar thermal degradation, consistent with that of the pure IL[73]. Based on the results, the addition of GNP did not impact the thermal stability of the INFs. The thermal degradation onset (T_Onset) observed at approximately 95 °C corresponds to the loss of water present in the [Emim] Ac INF, not the IL itself. [Emim] Ac exhibits a much higher thermal stability, with degradation occurring around 250 °C. This distinction is critical, as it highlights the ability of [Emim] Ac to function effectively in high-temperature applications beyond the range of water.

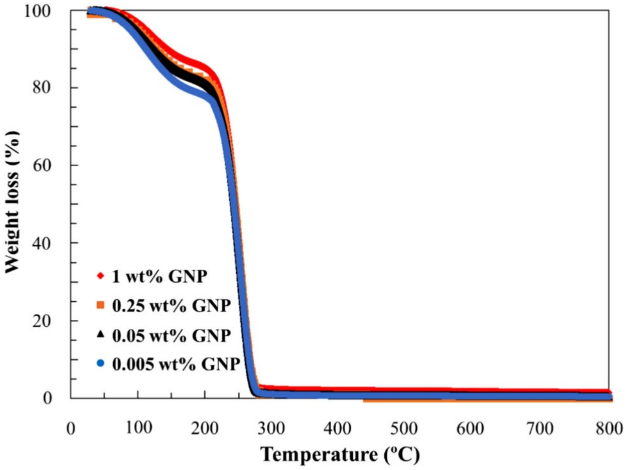

Fig. 12. Thermogravimetric analysis in inert atmosphere of the INFs.

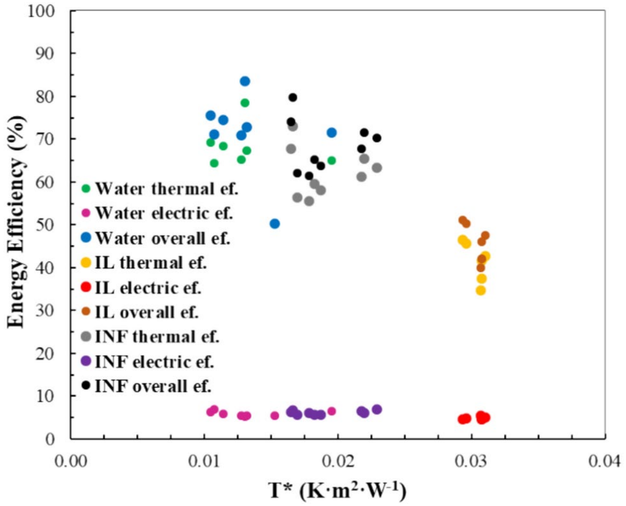

Fig. 13. Thermal, electric, and overall energy efficiency of the PVT solar collector.

	η_{therm} (%)	η_{elec} (%)	$\eta_{overall}$ (%)	$\eta_{ex,therm}$ (%)	$\eta_{ex,overall}$ (%)
Water	68.29	5.90	71.28	2.80	9.11
IL	41.40	4.81	46.21	2.78	7.93
INF	62.25	6.18	68.43	3.10	9.62

Table 3. Average efficiencies (%) of the PVT solar collector depending on the heat carrier fluid.

Solar collector tests

Among the prepared INFs, the INF containing a 1% mass fraction of GNP was selected to be used as thermal fluid in the PVT solar collector. This selection was based on its high stability, confirmed by DLS and TSI, as well as its high thermal conductivity, and high specific heat capacity, compared with the other INFs. For comparison purposes, tests were also conducted using water and IL as heat carrier fluids.

Figure 13 depicts the energy efficiency of the PVT collector as a function of the reduced temperature during the three tests and Table 3 shows the average efficiency of the PVT collector working with the three heat transfer fluids. As can be seen, the thermal, electric, and overall efficiency obtained with the INF and with water are of the same order, being the mean overall efficiency in the case of water a little higher than with the INF (average values of 71.28% vs. 68.43%), due to the higher thermal efficiency obtained with water (see Table 3). However, the use of INFs as heat carrier fluids has numerous advantages respect to water due to water is not feasible at high temperatures because it has a high vapour pressure and vaporizes above 100 °C at atmospheric pressure[31]. The results obtained with pure IL were significantly inferior, highlighting the positive effect of adding GNP to the IL.

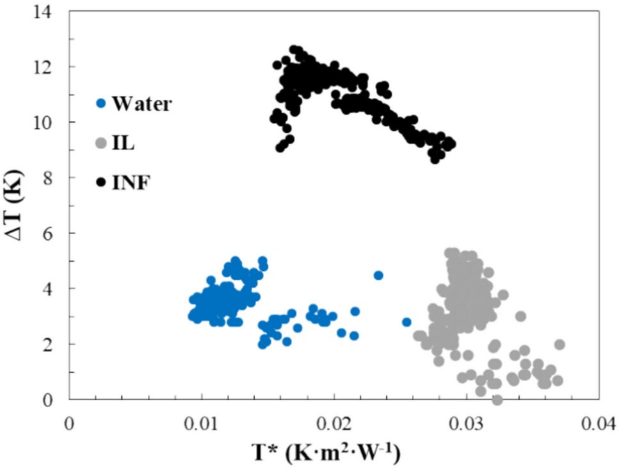

Fig. 14. The temperature rise of the heat carrier fluid in the PVT solar collector in 10–14 h UTC.

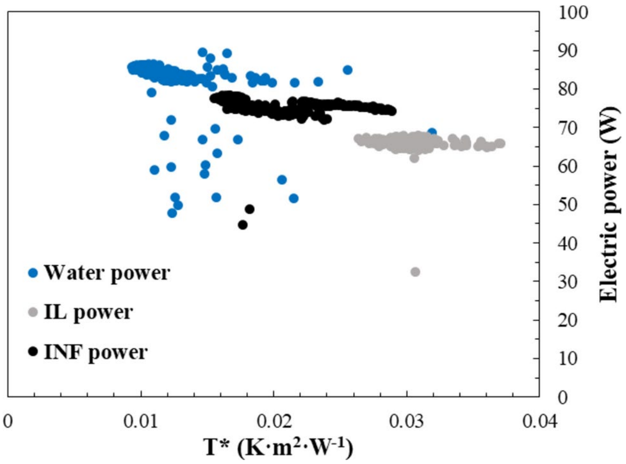

Fig. 15. Electric power generation of PVT solar collector depending on the heat carrier fluid in 10–14 h UTC.

The INF's performance, nearly matching that of water while offering extended operational range, demonstrates its potential as an advanced heat transfer fluid for PVT systems. This is particularly relevant for applications requiring higher operating temperatures or where water's limitations become problematic. The marked improvement of the INF over pure IL underscores the synergistic effect of GNP addition, likely due to enhanced thermal properties and stability. These findings suggest that further optimization of GNP concentration in INFs could lead to heat transfer fluids that surpass the performance of conventional options across a broader range of operating conditions.

Figure 14 illustrates the temperature rise of the heat transfer fluid inside the collector when using water, IL and INF. The results reveal a remarkable difference in thermal behavior between these fluids. The data clearly demonstrate that INF exhibits a significantly higher temperature increase compared to both IL alone and water, highlighting its superior thermal behavior. Specifically, the temperature rise with INF is approximately four times greater than that of water. This pronounced difference is primarily due to the lower specific heat capacity of the IL in the INF, which inherently absorbs less heat per unit mass compared to water[49]. Consequently, this allows the INF to achieve a much larger temperature jump, presenting several advantages for solar thermal applications[74]. Notably, the higher temperature rise enhances system efficiency by enabling quicker attainment of elevated operating temperatures, thereby boosting overall thermal performance. Additionally, the ability to reach higher temperatures broadens the range of applications for solar collectors, making them particularly suitable for processes that demand greater temperature input.

Figure 15 presents an interesting result regarding the electrical performance of the PVT system. It can be seen that, despite the large temperature difference of the fluids, the electrical performance of the PV cells is not greatly affected by the choice of the heat transfer fluid. This observation is particularly noteworthy since, not only theoretically but also according to the manufacturers, high temperatures decrease the electrical output of the PVT cells.

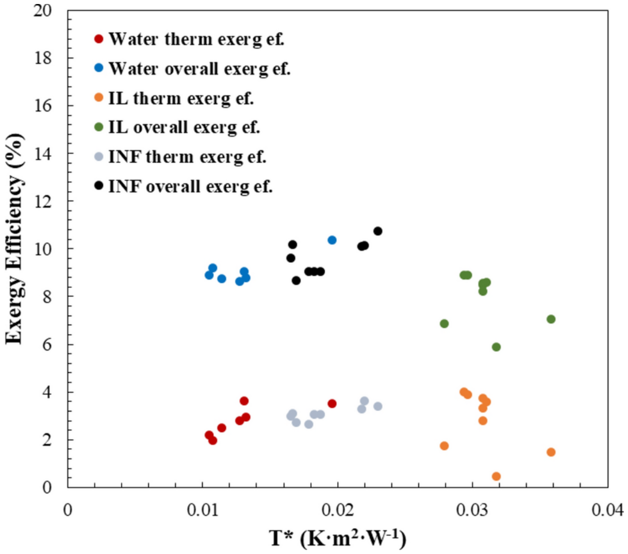

Fig. 16. Thermal and overall exergy efficiency of the PVT solar collector.

The exergy is a well-known thermodynamic variable that distinguishes among the qualities of the different types of energy. Unlike total energy, which measures only quantity, exergy considers the ability of an energy source to perform useful work, taking into account environmental constraints and irreversibilities[75,76]. The exergy analysis of a system is often referred as Second Law analysis and is preferred to compare energy magnitudes of different types, as is the case of PVT solar collectors[77,78]. Exergy is defined as the maximum useful work that can be extracted from an energy conversion process as it reaches equilibrium with the thermodynamic environment or dead state. This concept is crucial in assessing solar collectors of various types, including hybrid panels and those utilizing nanofluids[79,80]. In terms of this variable, the exergy increases of a fluid flow, Ex_{therm}, is given by Eq. (8) [81].

$$Ex_{therm} = \dot{m}\left[(h_{out} - h_{in}) - T_0\,(s_{out} - s_{in})\right] = \dot{m} \cdot c_p \left[(T_{out} - T_{in}) - T_{amb} \cdot ln\frac{T_{in}}{T_{out}}\right] \tag{8}$$

Being h and s enthalpy and entropy, respectively, and referring subscripts out and in the output and input sections, respectively. T_0 (K) is the so-called *dead* state temperature, which in this context has been considered as the ambient temperature, T_{amb}. In the case of the electric power, its exergy (Ex_{el}) has the same value of the electric energy, P, as seen in Eq. (9), because theoretically electrical energy can be transformed completely into work irrespective of the environment and is therefore considered of the highest quality[77].

$$Ex_{el} = P \tag{9}$$

For the purpose of assessing the exergy of the solar irradiance, Ex_{solar}, it can be considered as that emitted by a blackbody at $T_{irr} = 5777$ K[78] or the apparent sun temperature. Its value is given by Eq. (10)[77–79].

$$Ex_{solar} = G \cdot A_{col}\left[1 - \left(\frac{T_{amb}}{T_{irr}}\right)\right] \tag{10}$$

Therefore, the exergy efficiency of the heat generated in the solar collector, $\eta_{ex,therm}$, is given by Eq. (11).

$$\eta_{ex,therm} = \frac{Ex_{therm}}{Ex_{solar}} \tag{11}$$

Finally, the overall exergy efficiency of the hybrid collector, $\eta_{ex,overall}$, is assessed by the ratio of the process output and the process input, both expressed in terms of exergy[82] and is calculated by Eq. (12).

$$\eta_{ex,overall} = \frac{Ex_{therm} + Ex_{el}}{Ex_{solar}} \tag{12}$$

As can be seen from Eq. (8), the exergy of the thermal flows depends on their temperature[76]. As it has been discussed before, temperature T_{out} is higher when using INF as heat carrier, being the exergy of the INF thermal flow greater than that of water. Figure 16 represents the exergy efficiency of the PVT collector when using INF, IL, and water.

The low values of the exergy efficiency compared to energy efficiency (see also Table 3) may be striking for readers not used to working with exergy. They are a consequence of the high value of the solar radiation exergy given by Eq. (10), whose reference temperature, T_{irr}, is much higher than that of the working fluids in FPSC. This is not the case for electric power, which has maximum exergy rating as Eq. (9) shows. Consequently, the use of the exergy variable reduces the value of the thermal energy compared to the electric one, giving a more realistic view of the real importance of both types of energy.

As can be observed in Table 3, the exergy efficiency of PVT solar collector is higher when using the INF with an average value of 9.62% (black dots in Fig. 16) with respect to that obtained when using water with an average value of 9.11% (orange dots in Fig. 16), because of the higher thermal exergy reached by the collector due to the higher temperatures of the INF. This represents a 5.6% increase of the collector exergy efficiency when using INF instead of water, which means that the energy generated by the PVT solar collector is more valuable working with INF than with water. The results obtained by the IL are the lowest of the three heat carrier fluids, which is quite interesting, because it means that the GNP really improve the IL even surpassing that of the water.

On the other hand, is also remarkable that the behavior of the INF during the tests have been completely normal, not presenting important negative circumstances nor in the PVT solar collector or the rest of components of the solar plant nor to the INF itself, which have maintained the state of suspension quite well. The only noticeable consequence is that if changing the working fluid to another one, which is not normal in solar plant operation, some contamination of GNP can appear.

Conclusions

This study presents groundbreaking research on the application of INFs in commercial PVT solar collectors, marking the first known instance of testing ILs and their INF derivatives under real operating conditions in commercial devices.

Key findings

1. **INF Characterization**: Four INFs based on [Emim] Ac IL with varying GNP concentrations (1%, 0.25%, 0.05%, and 0.005%) were successfully produced and comprehensively characterized.
2. **Performance Comparison**:
- Energy Efficiency: INFs and water demonstrated comparable results in thermal and electric generation, with water slightly outperforming in thermal energy production.
- Temperature Increase: INFs exhibited a significantly higher temperature rise within the collector due to their lower specific heat capacity, without compromising electric generation.
- Exergy Efficiency: The collector's exergy efficiency increased by approximately 5% when using INFs with respect to the base fluid IL, a substantial improvement that broadens the potential applications of solar energy.
3. **IL Performance**: The pure IL showed the poorest performance among the three heat carrier fluids, highlighting the substantial improvement achieved by GNP addition.
4. **System Compatibility**: The use of INFs in the commercial collector revealed no significant drawbacks for the solar plant and showed no deterioration of the nanoparticle suspension.
5. **INF remains advantageous compared to water**: The low vapor pressure of [Emim] Ac minimizes evaporation losses, making it ideal for long-term use in open or high-temperature systems where water would suffer significant losses. Additionally, unlike water, which undergoes phase changes at 100 °C, [Emim] Ac remains in the liquid phase across a wider temperature range, avoiding issues such as latent heat losses or pressure increases within the system. Furthermore, [Emim] Ac ensures excellent dispersion stability for GNP, preventing aggregation and maintaining consistent thermophysical properties. This stability enhances long-term performance, outperforming water-based nanofluids that are prone to sedimentation.

Implications and future directions

The favorable results obtained from using INFs in solar collectors open new avenues for future research and applications. The enhanced exergy efficiency and higher temperature jumps achieved with INFs suggest their potential to expand the scope of solar energy applications, particularly in scenarios requiring higher operating temperatures. These findings underscore the promise of INFs as next-generation heat transfer fluids in solar thermal systems. Future research should focus on optimizing INF compositions, exploring their long-term stability and performance in various solar collector designs, and investigating their potential in other renewable energy applications.

Data availability

The data used to support the finding of this study are included within the article and its supplementary information files.

Received: 16 October 2024; Accepted: 18 February 2025

References

1. Mekhilef, S., Saidur, R. & Safari, A. A review on solar energy use in industries. *Renew. Sustain. Energy Rev.* **15**, 1777–1790 (2011).
2. Manisalidis, I., Stavropoulou, E., Stavropoulos, A. & Bezirtzoglou, E. Environmental and health impacts of air pollution: A review. *Front. Public Health* **8**, 1–13 (2020).
3. Sakhaei, S. A. & Valipour, M. S. Performance enhancement analysis of the flat plate collectors: A comprehensive review. *Renew. Sustain. Energy Rev.* **102**, 186–204 (2019).
4. Fath, B. D. & Fath, B. D. *Managing Air Quality and Energy Systems* (CRC Press, 2020).

5. Bazen, E. F. & Brown, M. A. Feasibility of solar technology (photovoltaic) adoption: A case study on Tennessee's poultry industry. *Renew. Energy* **34**, 748–754 (2009).
6. Kalogirou, S. A. Solar thermal collectors and applications. *Prog. Energy Combust. Sci.* **30**, 231 (2004).
7. Khanafer, K. & Vafai, K. A review on the applications of nanofluids in solar energy field. *Renew. Energy* **123**, 398–406 (2018).
8. Hu, G. et al. Potential evaluation of hybrid nanofluids for solar thermal energy harvesting: A review of recent advances. *Sustain. Energy Technol. Assess.* **48**, 101651 (2021).
9. Sheikholeslami, M., Farshad, S. A., Ebrahimpour, Z. & Said, Z. Recent progress on flat plate solar collectors and photovoltaic systems in the presence of nanofluid: A review. *J. Clean. Prod.* **293**, 126119 (2021).
10. Dincer, I. & Bicer, Y. *PV-Based Energy Conversion Systems* (Elsevier, 2018).
11. Ibrahim, A., Othman, M. Y., Ruslan, M. H., Mat, S. & Sopian, K. Recent advances in flat plate photovoltaic/thermal (PV/T) solar collectors. *Renew. Sustain. Energy Rev.* **15**, 352–365 (2011).
12. Aste, N., del Pero, C. & Leonforte, F. Water flat plate PV-thermal collectors: A review. *Solar Energy* **102**, 98–115 (2014).
13. Dupeyrat, P., Ménézo, C., Rommel, M. & Henning, H. M. Efficient single glazed flat plate photovoltaic-thermal hybrid collector for domestic hot water system. *Solar Energy* **85**, 1457–1468 (2011).
14. Vignarooban, K. et al. Vapor pressure and corrosivity of ternary metal-chloride molten-salt based heat transfer fluids for use in concentrating solar power systems. *Appl. Energy* **159**, 206–213 (2015).
15. Kondaiah, P. & Pitchumani, R. Progress and opportunities in corrosion mitigation in heat transfer fluids for next-generation concentrating solar power. *Renewable Energy* vol. 205 956–991 Preprint at https://doi.org/10.1016/j.renene.2023.01.044 (2023).
16. Zhao, C., Yan, J., Tian, X., Xue, X. & Zhao, Y. Progress in thermal energy storage technologies for achieving carbon neutrality. *Carbon Neutrality* **2**, (2023).
17. Gustaman Syarif, D., Izak Rudyardjo, D., Fisika Fakultas Sains dan Teknologi Universitas Airlangga Kampus Mulyorejo, D. C., Timur, J. & Sains dan Teknologi Nuklir Terapan Badan Tenaga Nuklir Nasional, P. *Synthesize and Characterization of Aluminum Oxide (Al 2 O 3) Nanoparticle from Aluminum Waste for Nano Fluid Application*. vol. 1 (2020).
18. Wang, X.-J., Li, X. & Yang, S. Influence of pH and SDBS on the stability and thermal conductivity of nanofluids. *Energy Fuels* **23**, 2684 (2009).
19. Akram, N. et al. A facile, green fabrication of aqueous nanofluids containing hydrophilic functionalized carbon nanotubes toward improving heat transfer in a closed horizontal flow passage. *Powder Technol.* **404**, 117451 (2022).
20. Akram, N. et al. Application of PEG-Fe3O4 nanofluid in flat-plate solar collector: An experimental investigation. *Solar Energy Mater. Solar Cells* **263**, 112566 (2023).
21. Singh, D. et al. Use of metallic nanoparticles to improve the thermophysical properties of organic heat transfer fluids used in concentrated solar power. *Solar Energy* **105**, 468–478 (2014).
22. Amar, M. et al. Energy, exergy and economic (3E) analysis of flat-plate solar collector using novel environmental friendly nanofluid. *Sci. Rep.* **13**, 1 (2023).
23. Akram, N. et al. An experimental investigation on the performance of a flat-plate solar collector using eco-friendly treated graphene nanoplatelets–water nanofluids. *J. Therm. Anal. Calorim.* **138**, 609–621 (2019).
24. Akram, N. et al. A comprehensive review on nanofluid operated solar flat plate collectors. *J. Therm. Anal. Calorim.* **139**, 1309–1343 (2019).
25. Chen, W., Zou, C. & Li, X. An investigation into the thermophysical and optical properties of SiC/ionic liquid nanofluid for direct absorption solar collector. *Solar Energy Mater. Solar Cells* **163**, 157–163 (2017).
26. Wang, F. et al. Surfactant-free ionic liquid-based nanofluids with remarkable thermal conductivity enhancement at very low loading of graphene. *Nanoscale Res. Lett.* **7**, 1–7 (2012).
27. Bakthavatchalam, B., Habib, K., Saidur, R., Saha, B. B. & Irshad, K. Comprehensive study on nanofluid and ionanofluid for heat transfer enhancement: A review on current and future perspective. *J. Mol. Liq.* **305**, 112787 (2020).
28. Minea, A. A. & Murshed, S. M. S. A review on development of ionic liquid based nanofluids and their heat transfer behavior. *Renew. Sustain. Energy Rev.* **91**, 584–599 (2018).
29. Zhang, F.-F., Zheng, F.-F., Wu, X.-H., Yin, Y.-L. & Chen, G. Variations of thermophysical properties and heat transfer performance of nanoparticle-enhanced ionic liquids. *R. Soc. Open Sci.* **6**, 182040 (2019).
30. Bo, L. et al. An overview of the applications of ionic fluids and deep eutectic solvents enhanced by nanoparticles. *J. Therm. Anal. Calorim.* **147**, 7589–7601 (2022).
31. Das, L. et al. State-of-the-art ionic liquid & ionanofluids incorporated with advanced nanomaterials for solar energy applications. *J. Mol. Liq.* **336**, 116563 (2021).
32. Diedrichs, A. & Gmehling, J. Measurement of heat capacities of ionic liquids by differential scanning calorimetry. *Fluid Phase Equilib.* **244**, 68–77 (2006).
33. Oster, K., Hardacre, C., Jacquemin, J., Ribeiro, A. P. C. & Elsinawi, A. Understanding the heat capacity enhancement in ionic liquid-based nanofluids (ionanofluids). *J. Mol. Liq.* **253**, 326–339 (2018).
34. Moens, L., Blake, D. M., Rudnicki, D. L. & Hale, M. J. Advanced thermal storage fluids for solar parabolic trough systems. *J. Solar Energy Eng. Trans. ASME* **125**, 112–116 (2003).
35. Asleshirin, S., Mazaheri, H., Omidkhah Nasrin, M. R. & Hassani Joshaghani, A. Investigation of thermophysical properties of Io nanofluids containing multi-walled carbon nanotubes and graphene. *Iran. J. Chem. Chem. Eng.* **41**, 380–391 (2022).
36. Hosseinghorbani, A., Mozaffarian, M. & Pazuki, G. Application of graphene oxide IoNanofluid as a superior heat transfer fluid in concentrated solar power plants. *Int. Commun. Heat Mass Transf.* **111**, 104450 (2020).
37. Sami, W., Kazi, S. N. & Badarudin, A. Thermal performance of a flat-plate solar collector using aqueous colloidal dispersions of graphene nanoplatelets with different specific surface areas. *Appl. Therm. Eng.* **25**, 115142 (2020).
38. Alawi, O. A., Kamar, H. M., Mohammed, H. A., Mallah, A. R. & Hussein, O. A. Energy efficiency of a flat-plate solar collector using thermally treated graphene-based nanofluids: Experimental study. *Nanomater. Nanotechnol.* **10**, 184798042096461 (2020).
39. Omrani, A. N., Esmaeilzadeh, E., Jafari, M. & Behzadmehr, A. Effects of multi walled carbon nanotubes shape and size on thermal conductivity and viscosity of nanofluids. *Diam. Relat. Mater.* **93**, 96–104 (2019).
40. Alawi, O. A. et al. Graphene nanoplatelets suspended in different basefluids based solar collector: An experimental and analytical study. *Processes* **9**, 1–22 (2021).
41. Alawi, O. A. et al. Experimental and theoretical analysis of energy efficiency in a flat plate solar collector using monolayer graphene nanofluids. *Sustainability (Switzerland)* **13**, 5416 (2021).
42. Park, S.-S., Han, S.-P., Jeon, Y.-H., Kim, J.-Y. & Kim, N.-J. A comparative study on the characteristics of nanofluids to the shape of graphene and carbon nanotube. *J. Korean Solar Energy Soc.* **33**, 99–106 (2013).
43. Thota, R., Biswas, A., Das, B. & Sengupta, A. R. Experimental investigation of solar evacuated tube collector with multi-walled carbon nanotube-water-based nanofluid. *Energy Sour. A: Recov. Util. Environ. Effects* **45**, 924–939 (2023).
44. Lingala, S. S. Ionic-liquid-based nanofluids and their heat-transfer applications: A comprehensive review. *ChemPhysChem* vol. 24. Preprint at https://doi.org/10.1002/cphc.202300191 (2023).
45. Abdullatif Alshuhail, L., Shaik, F. & Syam Sundar, L. Thermal efficiency enhancement of mono and hybrid nanofluids in solar thermal applications—A review. *Alex. Eng. J.* **68**, 365–404 (2023).
46. Aissa, A. et al. A review of the enhancement of solar thermal collectors using nanofluids and turbulators. *Appl. Therm. Eng.* **220**, 119663 (2023).

47. Das, L. et al. Improved thermophysical properties and energy efficiency of aqueous ionic liquid/mxene nanofluid in a hybrid pv/t solar system. *Nanomaterials* **10**, 1–26 (2020).
48. Shaik, N. B. et al. Artificial neural network modeling and optimization of thermophysical behavior of MXene Ionanofluids for hybrid solar photovoltaic and thermal systems. *Therm. Sci. Eng. Prog.* **33**, 101391 (2022).
49. Moulefera, I. *et al.* Novel application for graphene oxide-based ionanofluids in flat plate solar thermal collectors. *Sci. Rep.* **14**, (2024).
50. Montalbán, M. G., Hidalgo, J. M., Collado-González, M., Díaz Baños, F. G. & Víllora, G. Assessing chemical toxicity of ionic liquids on *Vibrio fischeri*: Correlation with structure and composition. *Chemosphere* **155**, 405–414 (2016).
51. *User Guide, Turbiscan Formulation Scientific Instrument*. (2018).
52. Seco-Nicolás, M., Alarcón, M. & Luna-Abad, J. P. 3D numerical simulation of laminar forced-convection flow subjected to asymmetric thermal conditions. An application to solar thermal collectors. *Solar Energy* **220**, 230–245 (2021).
53. ENDEF Solar Solutions. Panel Solar Híbrido ECOMESH. https://endef.com/panel-solar-hibrido/ecomesh/.
54. AENOR UNE-EN 12975. *Captadores Solares. Requisitos Generales* (2022).
55. *Solar Engineering of Thermal Processes: J A Duffie and W A Beckman Wiley (1980) 762 pp. Design Studies* vol. 3 (1982).
56. Gagliano, A., Tina, G. M., Aneli, S. & Nižetić, S. Comparative assessments of the performances of PV/T and conventional solar plants. *J. Clean. Prod.* **219**, 304–315 (2019).
57. Zayed, M. E., Zhao, J., Du, Y., Kabeel, A. E. & Shalaby, S. M. Factors affecting the thermal performance of the flat plate solar collector using nanofluids: A review. *Solar Energy* **182**, 382–396 (2019).
58. Said, Z. et al. Recent advances on nanofluids for low to medium temperature solar collectors: energy, exergy, economic analysis and environmental impact. *Prog. Energy Combust. Sci.* **84**, 100898 (2021).
59. Ota, J., Hait, S. K., Sastry, M. I. S. & Ramakumar, S. S. V. Graphene dispersion in hydrocarbon medium and its application in lubricant technology. *RSC Adv.* **5**, 53326–53332 (2015).
60. Jyotsna Kalpana, V. et al. Preparation and experimental investigations on the mechanical behavior of hybrid polymer nanocomposite with boron carbide and graphene nanoplatelets. *Cogent. Eng.* **11**, 1 (2024).
61. Wei, J., Atif, R., Vo, T. & Inam, F. Graphene nanoplatelets in epoxy system: dispersion, reaggregation, and mechanical properties of nanocomposites. *J. Nanomater.* **2015** (2015).
62. Raji, M., Essabir, H., Rodrigue, D., Bouhfid, R. & Qaiss, A. el kacem. Influence of graphene oxide and graphene nanosheet on the properties of polyvinylidene fluoride nanocomposites. *Polym. Compos.* **39**, 2932–2941 (2018).
63. Thomas, D.-G., Kavak, E., Hashemi, N., Montazami, R. & Hashemi, N. N. Synthesis of graphene nanosheets through spontaneous sodiation process. *C (Basel)* **4**, 42 (2018).
64. Neelgund, G. M., Oki, A. & Luo, Z. In situ deposition of hydroxyapatite on graphene nanosheets. *Mater. Res. Bull.* **48**, 175–179 (2013).
65. López, T.D.-F. et al. Engineered silica nanoparticles as additives in lubricant oils. *Sci. Technol. Adv. Mater.* **16**, 55005 (2015).
66. Li, Z. et al. Topical application of silk fibroin-based hydrogel in preventing hypertrophic scars. *Colloids Surf. B Biointerfaces* **186**, 110735 (2020).
67. Sunatkari, A. L., Talwatkar, S. S., Tamgadge, Y. S. & Muley, G. G. Comprehensive study of L-Alanine passivated colloidal gold nanoparticles and GNP-PVP thin films: Linear optical properties and very large nonlinear refractive index, absorption coefficient, third-order nonlinear susceptibility measurements and effect of passivation. *Opt. Mater. (Amst.)* **121**, (2021).
68. Anin Vincely, D. & Natarajan, E. Experimental investigation of the solar FPC performance using graphene oxide nanofluid under forced circulation. *Energy Convers. Manag.* **117**, 1–11 (2016).
69. Yu, W., Xie, H., Chen, L. & Li, Y. Investigation of thermal conductivity and viscosity of ethylene glycol based ZnO nanofluid. *Thermochim Acta* **491**, 92–96 (2009).
70. Bao, J., Heyd, R., Régnier, G., Ammar, A. & Peixinho, J. Viscosity of graphene in lubricating oil, ethylene glycol and glycerol. *J. Therm. Anal. Calorim.* **148**, 11455–11465 (2023).
71. Shahzad, A. *Impact of Thermal Conductivity on Energy Technologies*, 57–67 (IntechOpen, 2018).
72. Wang, B., Wang, X., Lou, W. & Hao, J. Gold-ionic liquid nanofluids with preferably tribological properties and thermal conductivity. *Nanoscale Res Lett* **6**, 2–11 (2011).
73. Zaitsau, D. H., Papusha, M., Kopp, W. A. & Leonhard, K. Thermal decomposition of 1-ethyl-3-methylimidazolium acetate. *J, Mol, Liq,* **390**, 123093 (2023).
74. Zhang, F. F. et al. Thermophysical properties and water sorption characteristics of 1-ethyl-3-methylimidazolium acetate ionic liquid and water binary systems. *Int. Commun. Heat Mass Transf.* **127**, 105558 (2021).
75. Moran, M. J. & Shapiro, H. N. *Fundamentals of Engineering Thermodynamics* (Wiley, 2006).
76. Bejan, A. *Advanced Engineering Thermodynamics* (Wiley, 2016).
77. Kazemian, A. et al. Energy, exergy and environmental analysis of glazed and unglazed PVT system integrated with phase change material: An experimental approach. *Solar Energy* **201**, 178–189 (2020).
78. Li, M., Zhong, D., Ma, T., Kazemian, A. & Gu, W. Photovoltaic thermal module and solar thermal collector connected in series: Energy and exergy analysis. *Energy Convers. Manag.* **206**, 112479 (2020).
79. Özakın, A. N. & Kaya, F. Experimental thermodynamic analysis of air-based PVT system using fins in different materials: Optimization of control parameters by Taguchi method and ANOVA. *Solar Energy* **197**, 199–211 (2020).
80. Shojaeizadeh, E. & Veysi, F. Development of a correlation for parameter controlling using exergy efficiency optimization of an Al_2O_3/water nanofluid based flat-plate solar collector. *Appl. Therm. Eng.* **98**, 1116–1129 (2016).
81. Said, Z., Saidur, R. & Rahim, N. A. Energy and exergy analysis of a flat plate solar collector using different sizes of aluminium oxide based nanofluid. *J. Clean. Prod.* **133**, 518–530 (2016).
82. Petela, R. Exergy of undiluted thermal radiation. *Solar Energy* **74**, 469–488 (2003).

Acknowledgements

Imane Moulefera acknowledges support from Spanish Ministry of Universities under "Margarita Salas program", financed by Next Generation EU.

Author contributions

I.M.: Conceptualization, Methodology, Investigation, Writing—original draft. J.J.: Investigation, Writing-Review and editing. A.C.: Methodology and Investigation. M.G.—review and editing. M.A.: Conceptualization, Writing—review and editing. G.V.: Conceptualization, Supervision, Project administration, Funding. All authors discussed the results and commented on the manuscript. All authors have read and agreed to the published version of the manuscript.

Funding

This work has been partially supported by Grants ref. TED2021-130389B-C21, PID2020-113081RB-I00 and

PID2023-150761OB-C21 funded by MCIN/AEI/ https://doi.org/10.13039/501100011033 and by EU ¨Next Generation¨, and part of the grant ref. 22129-PI-22 funded by the research support program of the Seneca Foundation of Science and Technology of Murcia, Spain. Imane Moulefera acknowledges support from Spanish Ministry of Universities under "Margarita Salas program", financed by Next Generation EU.

Declarations

Competing interests

The authors declare no conflict of interest.

Additional information

Supplementary Information The online version contains supplementary material available at https://doi.org/10.1038/s41598-025-91040-w.

Correspondence and requests for materials should be addressed to J.J.D.M.

Reprints and permissions information is available at www.nature.com/reprints.